

Impact of Lithium Sources on Growth Process and Structural Stability of Single-Crystalline Li-Rich Layered Cathodes

Jing Ai⁺^[a], Xiaowen Zhao⁺^[a], Xin Cao,^{*[a]} Lin Xu,^[a] Ping Wu,^{*[a]} Yiming Zhou,^[a] Ping He,^[b] Yawen Tang,^[a] and Haoshen Zhou^{*[b]}

Single-crystalline (SC) Li-rich layered oxides have garnered significant attention due to their inhibited lattice oxygen release and reduced crack formation compared with polycrystalline (PC) counterparts. However, it raises a crucial question regarding the selection of prevailing lithium sources-Li₂CO₃ and LiOH·H₂O-for the solid-state synthesis of SC cathodes, which critically impacts the technical route and future development of SC materials. Herein, a series of SC Li-rich layered cathodes were synthesized using these two lithium sources. The SC materials prepared with LiOH·H₂O (LRO-H) exhibited larger grain sizes compared with those using Li₂CO₃ (LRO-C). This can be attributed to the lower phase transition temperature of the

precursor to spinel phase, which promotes further SC growth during solid-state reactions. Furthermore, LRO-H demonstrated excellent electrochemical stability, whereas LRO-C exhibited superior initial capacities. To balance these attributes, a mixed lithium sources system (LRO-M) was proposed, showing superior Li⁺ diffusion kinetics and suppressed layered-to-spinel transformation, resulting in excellent rate performance and an extended battery lifespan. Altogether, these findings provide critical insights into the impact of lithium sources on the growth process, structural stability, and electrochemical properties of SC Li-rich layered cathodes, guiding the synthesis and design of next-generation cathode materials.

Introduction

Due to the increasing requirements on high energy density by numerous industries such as electric vehicles, consumer electronics products, and energy storage devices, the development of high-performance Li-ion batteries is imminent.^[1–5] As an indispensable component, the cathode material directly influences the energy storage ability of lithium-ion battery. However, currently commercial cathode materials such as LiCoO₂, LiNi_xCo_yMn_{1-x-y}O₂, LiFePO₄, etc. are unable to overcome energy bottleneck, which seriously limits the development of Li-ion batteries due to capacity mismatch with anodes such as hard carbon and Si/C anodes.^[6–12] It is worth noting that Li-rich layered oxide materials have received increasing attention in recent years, exhibiting high operating potential and superior output capacity (> 250 mAh g⁻¹), which can be attributed to its

unique charge mechanism based on simultaneous cationic and oxygen-related anionic redox reaction.^[13,14] In physics, single-crystal refers to a type of material where the atoms are arranged in a highly ordered, repeating pattern extending throughout the entire structure. In contrast, in the field of battery materials, single-crystalline is generally considered to be the morphology with non-aggregated monodisperse primary particles, which is different from polycrystalline consisted of spherical secondary particles. Moreover, traditional Li-rich layered cathodes displayed the PC morphology, which always suffer from serious interface side reaction between electrode and electrolyte, further resulting in intergranular cracking and inferior layered/spinel phase transition, which eventually aggregates both capacity and voltage degradation.^[15]

Recent efforts confirmed the SC design can be regarded as a promising strategy for high-performance Li-rich layered oxides, which can directly avoid intergranular cracking and suppress stress concentration during charging/discharging process.^[16–19] Moreover, SC Li-rich layered cathodes displayed repressed oxygen loss, improved layered structure stability and superior electrochemical performances, which is beneficial to overcome and address the bottleneck faced by Li-rich cathodes. Furthermore, solid-state reaction can be conducted as a traditional approach for the synthesis of SC Li-rich layered oxides, which has numerous merits such as simple process and low energy consumption compared with other methods, like molten salt assisted and solvothermal methods.^[20–24] However, the choices of different Li sources during the synthesis process and their impact on the growth process of layered structure and corresponding electrochemical performance are unclear, which is required to further exploration. Therefore, optimizing reaction

[a] J. Ai,⁺ X. Zhao,⁺ X. Cao, L. Xu, P. Wu, Y. Zhou, Y. Tang
Jiangsu Collaborative Innovation Center of Biomedical Functional Materials,
Jiangsu Key Laboratory of New Power Batteries, Nanjing Normal University,
Nanjing 210023 (P. R. China)
E-mail: xincao@njnu.edu.cn
zjuwuping@njnu.edu.cn

[b] P. He, H. Zhou
Center of Energy Storage Materials & Technology, College of Engineering
and Applied Sciences, Jiangsu Key Laboratory of Artificial Functional
Materials National Laboratory of Solid State Microstructures, Collaborative
Innovation Center of Advanced Microstructures, Nanjing University, Nanjing
210093 (P. R. China)
E-mail: hszhou@nju.edu.cn

[+] These authors contribute equally to this work.

Supporting information for this article is available on the WWW under
<https://doi.org/10.1002/batt.202400425>

conditions especially selecting suitable Li source is needed to guide the synthesis, which is beneficial to improve structural and electrochemical stability.

Herein, three kinds of SC Li-rich layered materials, $\text{Li}_{1.2}\text{Ni}_{0.13}\text{Co}_{0.13}\text{Mn}_{0.54}\text{O}_2$, were prepared by selecting different Li source during solid-state synthesis at high temperature, in which Li_2CO_3 , the mixture of Li_2CO_3 and $\text{LiOH}\cdot\text{H}_2\text{O}$ with a molar ratio of 1:1 as well as $\text{LiOH}\cdot\text{H}_2\text{O}$ were mixed with the transition metal (TM) precursor, respectively. Moreover, we found the mixed Li salts (Li_2CO_3 and $\text{LiOH}\cdot\text{H}_2\text{O}$) can be acted as the optimized Li source compared with others, thus activated lithiation reaction with the beginning of $\sim 300^\circ\text{C}$ and optimized particle size of 759 nm can be obtained in the LRO-M, which further results in high crystallinity of the product and rapid Li^+ diffusion kinetics. Furthermore, excellent cycle stability and rate performance can be achieved in the LRO-M with the retention of 84.4% upon 300 cycles, still reaching 104.8 mAh g^{-1} at 5 C, which exhibits superior Li^+ diffusion kinetics with the maximum diffusion coefficient of $1.7 \times 10^{-10} \text{ cm}^2 \text{s}^{-1}$. Besides, inferior layered/spinel phase transition can be effectively suppressed within LRO-M, in sharp contrast to the LRO-C and the LRO-H,

further indicating stable layered structure can be maintained within the LRO-M.

Results and Discussion

X-ray diffraction (XRD) and corresponding refinement results with relatively reliable fitting values (Table S1-3) revealed all samples assign to the layered structure with $R-3m$ and $C2/m$ space groups (Figure 1a-c), where a series of weak peaks in the 2θ range of $20\text{--}30^\circ$ response to Li/Mn ordered arrangement in the TM layer, which can be attributed to the occupation of TM sites in TM layer by extra Li.^[25,26] Besides, obviously divisive (006)/(012) and (018)/(110) peaks indicated all samples harvested superior layered structure. Moreover, the full width at half maximum (FWHM) of (020) superlattice peaks of three samples reflected the size of Li_2MnO_3 domain can be appropriately adjusted by using different Li sources (Figure S1), where LRO-M delivered the modest size in comparison to others.^[27-29] Furthermore, refinement results indicated that continuous decreases of the proportions of Li_2MnO_3 domain within the whole structure from LRO-C to LRO-M, and to LRO-H (Figure S2),

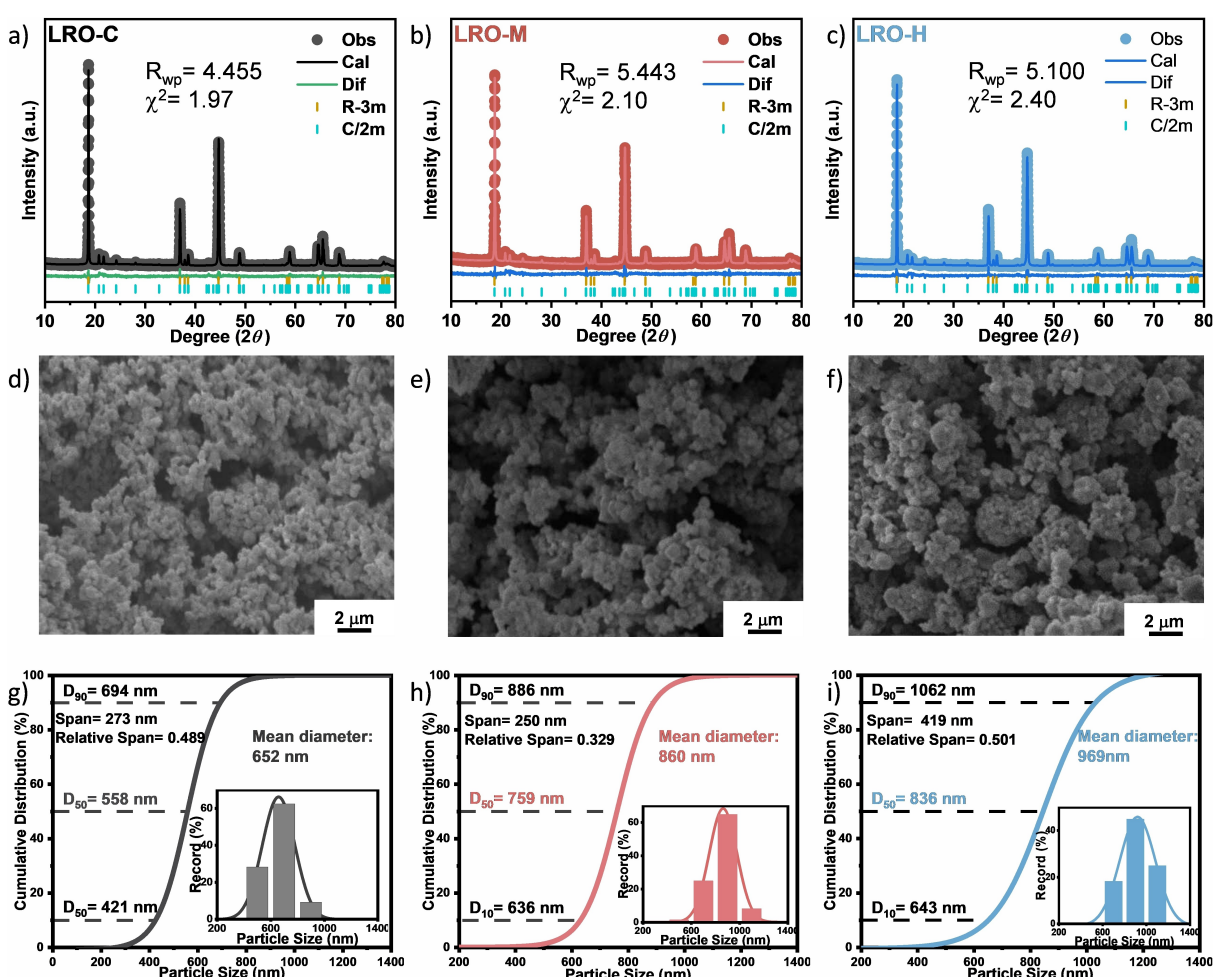


Figure 1. XRD patterns and refinement results of the a) LRO-C, b) LRO-M and c) LRO-H. SEM images of the d) LRO-C, e) LRO-M and f) LRO-H. Cumulative distribution curves of the g) LRO-C, h) LRO-M and i) LRO-H (particle size distributions, quartile diameters include D_{90} , D_{50} and D_{10} , mean diameters, spans and relative spans are listed in inserts).

which could further influence their electrochemical properties. In addition, scanning electron microscopy (SEM) was utilized to analyze the effect of Li source on the morphologies of Li-rich layered oxides, in which all samples exhibited SC morphologies composed of irregular primary particles (Figures 1d-f, S3 and S4). Nevertheless, primary grains displayed a tendency of agglomeration with the introduction of LiOH·H₂O acted as Li source (Figure 1e and f). Besides, LRO-C displayed relatively small particles with D₅₀ of 558 nm and uniform distribution with relative span ((D₉₀/D₁₀)/D₅₀) of 0.489 (Figure 1g). When utilizing LiOH·H₂O acted as partial Li source during synthesis process, relatively increasing particles with D₅₀ of 759 nm and a decreasing relative span of 0.329 were displayed in LRO-M (Figure 1h), which demonstrated the replacement of Li source undoubtedly influence the growth process of Li-rich layered oxides. Besides, LRO-H exhibited the largest particle size and inhomogeneous distribution with D₅₀ of 836 nm and a relative span of 0.501 (Figure 1i), which was consistent with SEM results. The above results indicated the particle size grows as the proportion of LiOH·H₂O increases, which might be ascribed to relatively early nucleation and subsequent growth process during solid-state growth process owing to the lower melting point of LiOH·H₂O (~460 °C) than Li₂CO₃ (~730 °C). In particular, LiOH·H₂O acted as Li source can create a molten solution

system during the pre-lithiation process at relatively low temperature (150~200 °C), accelerating lithiation reaction and particle growth during calcination, which further results in excessive growth of particles as well as agglomeration.^[30,31] Whereas, excessive large size of primary grains was not beneficial to Li⁺ diffusion kinetics, which might unavoidably limit output capacity and rate capability of Li-rich layered cathodes.^[32,33] Thus, the mixture of Li₂CO₃ and LiOH·H₂O can be regarded as an excellent choice to optimize the speed of both lithiation reaction and particle growth, delivering uniform and dispense SC grains, which not only obtained the layered structure with good crystallinity, but can achieve the balance between solid state Li₂CO₃ with partial molten solution offered by LiOH·H₂O.

To further reveal the influence of various types of Li sources on the phase evolution of SC Li-rich layered cathodes during calcination process, *ex-situ* XRD was carried out to characterize corresponding samples at different calcination stages. Previous efforts support the formation of Li-rich layered cathode, Li_{1-x}T_xMO₂ (TM=Ni, Co, Mn), with the hexagonal R-3 m and monoclinic C2/m space groups undergoes a intermediate product, Li_{1-x}T_{x+2}O₄ with the Fd-3 m space group from the TM hydroxide precursor (P-3 m1).^[34-36] Firstly, a series of diffraction peaks were observed in LRO-C sample at 25 °C (Figure 2a),

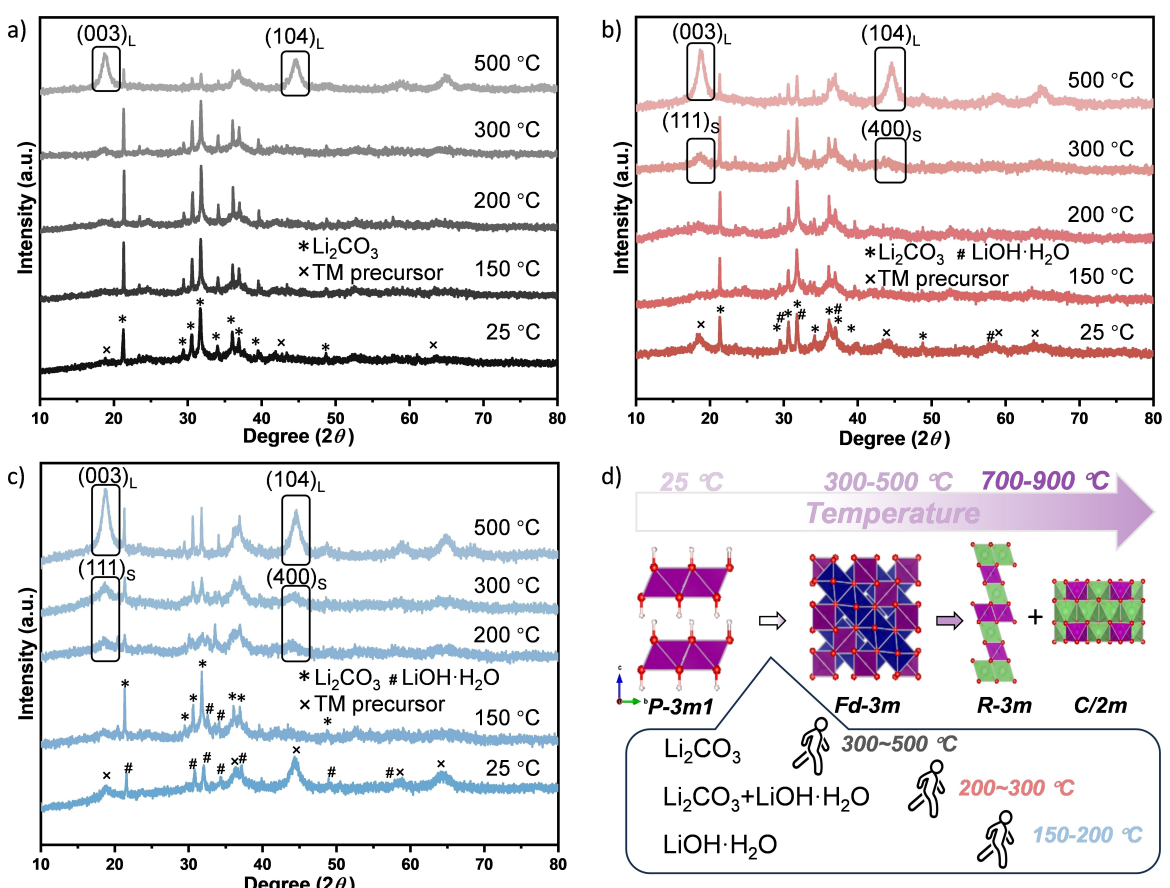


Figure 2. *Ex-situ* XRD patterns of the a) LRO-C, b) LRO-M and c) LRO-H during solid-state calcination process. d) Schematic diagram of phase transitions in the LRO during synthesis process and corresponding transition temperatures of the LRO-C, LRO-M and LRO-H with the Li sources of Li₂CO₃, the mixture of Li₂CO₃ and LiOH·H₂O (mol ratio=1:1) and LiOH·H₂O, respectively.

which can be indexed by the TM hydroxide precursor ($P-3m$ space group) and Li_2CO_3 . At 300°C , a single peak at around 18.5° can be slightly observed, while it is difficult to precisely infer that whether the spinel phase occurs. When it comes to 500°C , the main Bragg reflections of layered structure ((003) and (104) peaks) became dominant in the LRO-C sample with successive Li/O incorporation, which might be attributed to the generation of spinel phase and subsequently transform into layered structure in the temperature range of $300\text{--}500^\circ\text{C}$. When altering the Li source from pure Li_2CO_3 to the mixture of Li_2CO_3 and $\text{LiOH}\cdot\text{H}_2\text{O}$, the characteristic peaks can correspond to two kinds of Li salts and TM precursor at pristine state (25°C) (Figure 2b). It is worth noting that the (111) and (400) peaks of spinel $\text{Li}_{1-x}\text{TM}_{2+x}\text{O}_4$ with $Fd-3m$ space group can be observed when the temperature reached to 300°C , demonstrating the beginning of lithiation reaction and subsequent phase transition were activated by the incorporation of $\text{LiOH}\cdot\text{H}_2\text{O}$. In case of pure $\text{LiOH}\cdot\text{H}_2\text{O}$ as the Li source (Figure 2c), a series of characteristic peaks of Li_2CO_3 can be observed at 150°C , which can be ascribed to the reaction between dehydrated $\text{LiOH}\cdot\text{H}_2\text{O}$ with CO_2 . Moreover, (111) and (400) peaks belonged to $\text{Li}_{1-x}\text{TM}_{2+x}\text{O}_4$ intermediate product started to emerge at 200°C , presenting an obviously lower phase transitional temperature

compared with LRO-C and LRO-M samples. Even at 300°C , such intermediate product further increased as $\text{LiOH}\cdot\text{H}_2\text{O}$ continuous consuming, which certified that $\text{LiOH}\cdot\text{H}_2\text{O}$ reacted with TM precursor at lower temperature. Besides, the (003) and (104) peaks can be observed at 500°C , indicating the formation of layered structure. The above results further indicated different Li sources can obviously influence the lithiation speed and the temperature of phase transition during solid-state synthesis process (Figure 2d), which is beneficial to rationally adjust the growth process of Li-rich layered oxides for high-performance cathodes.

Further investigation was used to evaluate the electrochemical performances of Li-rich cathodes prepared by different Li sources, the electrodes were integrated into Li-half coin cells, testing at a current density of 20 mA g^{-1} with the voltage range of $2\text{--}4.8\text{ V}$ (Figure 3a-c). The initial charge profiles of three electrodes displayed slope regions assigned to TM oxidation and long plateau regions ($\sim 4.5\text{ V}$) belonged to oxygen-related anionic redox reaction, which was similar to reported Li-rich layered cathodes in previous research.^[37-41] Notably, the charging capacities based on lattice oxygen oxidation at around 4.5 V decreased during initial charging process, from LRO-C (259.0 mAh g^{-1}) to LRO-M (189.6 mAh g^{-1}), and to LRO-H

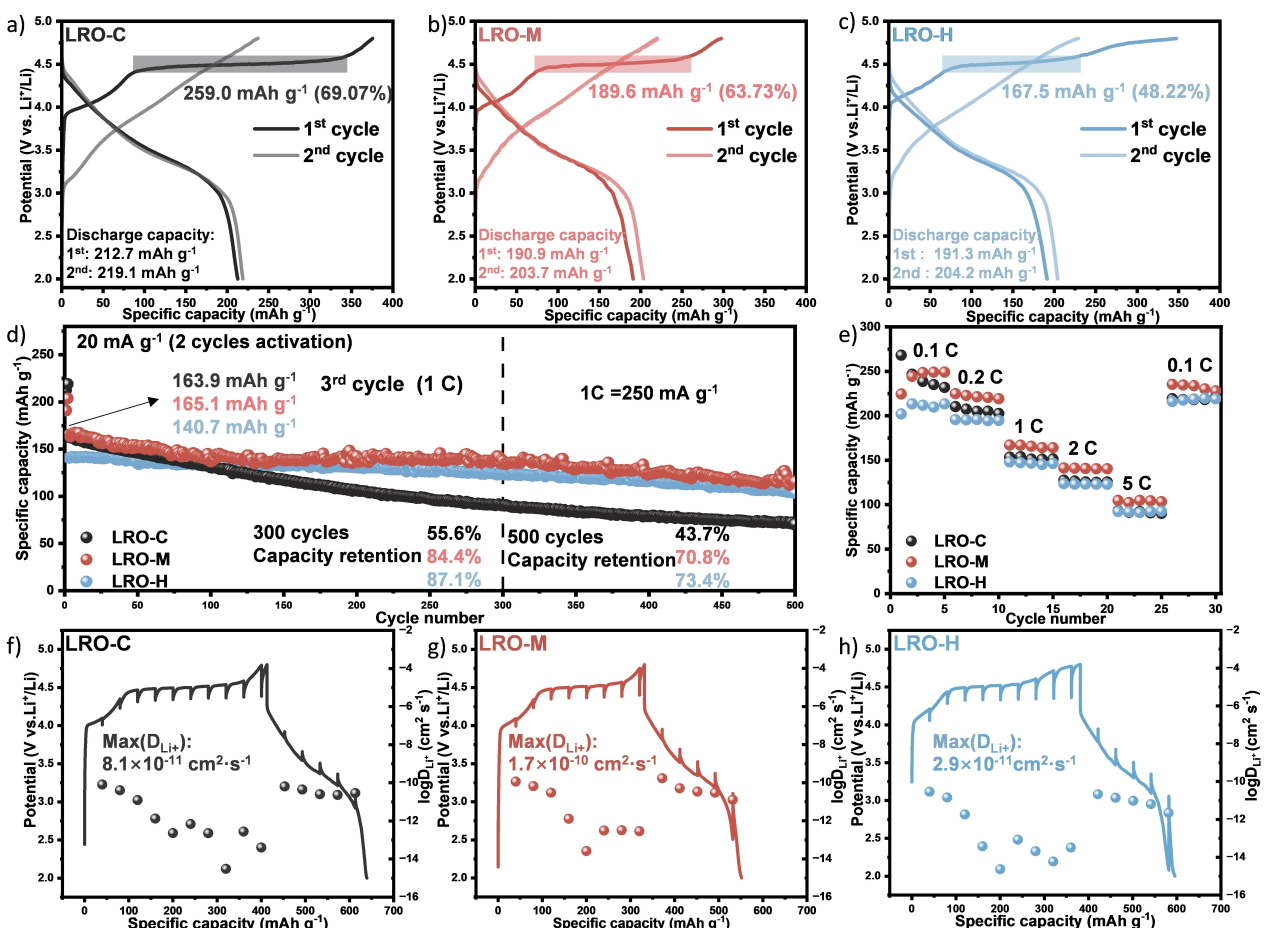


Figure 3. The initial two charging and discharging curves of the a) LRO-C, b) LRO-M and c) LRO-H at 20 mA g^{-1} . d) Cycle performances of samples with the voltage range of $2\text{--}4.8\text{ V}$ at 1 C (2 cycles activation at 20 mA g^{-1}). e) Rate performances of three cathodes at 0.1, 0.2, 1, 2 and 5 C. GITT curves and corresponding Li^{+} diffusion coefficients of the f) LRO-C, g) LRO-M and h) LRO-H.

(167.5 mAh g⁻¹), and their ratios in the total charging capacities were 69.07%, 63.73% and 48.22%, respectively. This might due to samples had different particle sizes, which causing various specific surface areas. LRO-C sample owned the largest specific surface area, which contacted with more electrolyte and activated more lattice oxygen oxidation reaction, resulting in high charge capacity. The specific surface areas of the LRO-M and LRO-H samples gradually decreased, bringing the gradual decrease in oxygen-related capacities. Furthermore, LRO-H electrode showed the extra capacity over the long plateau, which might contribute to the fact that LRO-H exhibited a crystal orientation, leading to the decomposition of electrolyte under high voltage (Figure S5). Moreover, the reversible discharge capacities are 212.7, 190.9 and 191.3 mAh g⁻¹ obtained from LRO-C, LRO-M and LRO-H, respectively. Furthermore, they delivered nearly discharge capacities of 219.1, 203.7 and 204.2 mAh g⁻¹, respectively, upon the second cycle. Moreover, the cycling performances of all samples were tested at 1 C (1 C = 250 mA g⁻¹) after two cycles activation, in which both LRO-M and LRO-H delivered relatively superior cycle stability with the capacity retention of 84.4% and 87.1%, respectively after 300 cycles, and 70.8% and 73.4%, respectively upon 500 cycles (Figure 3d). Nevertheless, LRO-H electrode exhibited the lower discharge capacity of 140.7 mAh g⁻¹ at 1 C, in comparison to the LRO-C and the LRO-M at the same condition, which delivered the discharge capacity of 163.9, 165.1 mAh g⁻¹, respectively. Such result might be ascribed to relatively slow Li⁺ diffusion kinetics owing to large particle size and agglomeration of the LRO-H. Furthermore, serious capacity fading with the retention of 55.6% can be observed within LRO-C upon 300 cycles, which also delivered only 43.7% after 500 cycles. Besides, the rate performances of three electrodes were investigated in Li-half cells at different current densities, in

which LRO-M displayed improved rate performance with discharge capacity of 249.2, 224.9, 167.1, 141.3 and 104.8 mAh g⁻¹ at 0.1, 0.2, 1, 2 and 5 C, respectively (Figure 3e). The above results demonstrated different Li sources can directly influence both the layered structure and electrochemical stability, where accelerated lithiation reaction and grain growth are beneficial to storage ability by the proper introduction of LiOH·H₂O. Besides, galvanostatic intermittent titration technique (GITT) was utilized to further evaluate Li⁺ diffusion kinetics upon charging/discharging process (Figure 3f-g). In particular, the maximum diffusion coefficient of 1.7×10⁻¹⁰ cm²s⁻¹ can be achieved in the LRO-M during the initial cycle, which further confirmed proper Li source is beneficial to improve dynamics performances of Li-rich layered cathodes. In contrast, the LRO-H exhibited relatively poor Li⁺ diffusion kinetics with the maximum diffusion coefficient of merely 2.9×10⁻¹¹ cm²s⁻¹, which could be attributed to large particle size and agglomerate morphology. In addition, the LRO-C obtained the maximum diffusion coefficient of 8.1×10⁻¹¹ cm²s⁻¹ at the same condition. The above results supported the mixture of LiOH·H₂O and Li₂CO₃ can be regarded as the proper Li source during solid-state synthesis, which effectively enhances both cycle stability and Li⁺ diffusion kinetics of Li-rich layered cathodes.

Besides, the structural stabilities of the LRO-C, LRO-M and LRO-H cathodes were examined via Raman spectroscopy (Figure 4a-c). Three samples exhibited similar spectra profiles at the pristine states, where two obvious peaks at approximately 600 cm⁻¹ and 483 cm⁻¹, respectively, can be assigned to layered structure LiTMO₂ with the *R*-3*m* space group, and an additional peak at approximately 425 cm⁻¹ belongs to the monoclinic Li₂MnO₃ with the *C*/2*m* space group. Moreover, the signals of both the LiTMO₂ and Li₂MnO₃ can be observed in three samples upon 500 cycles, which proved all cathodes possess stable

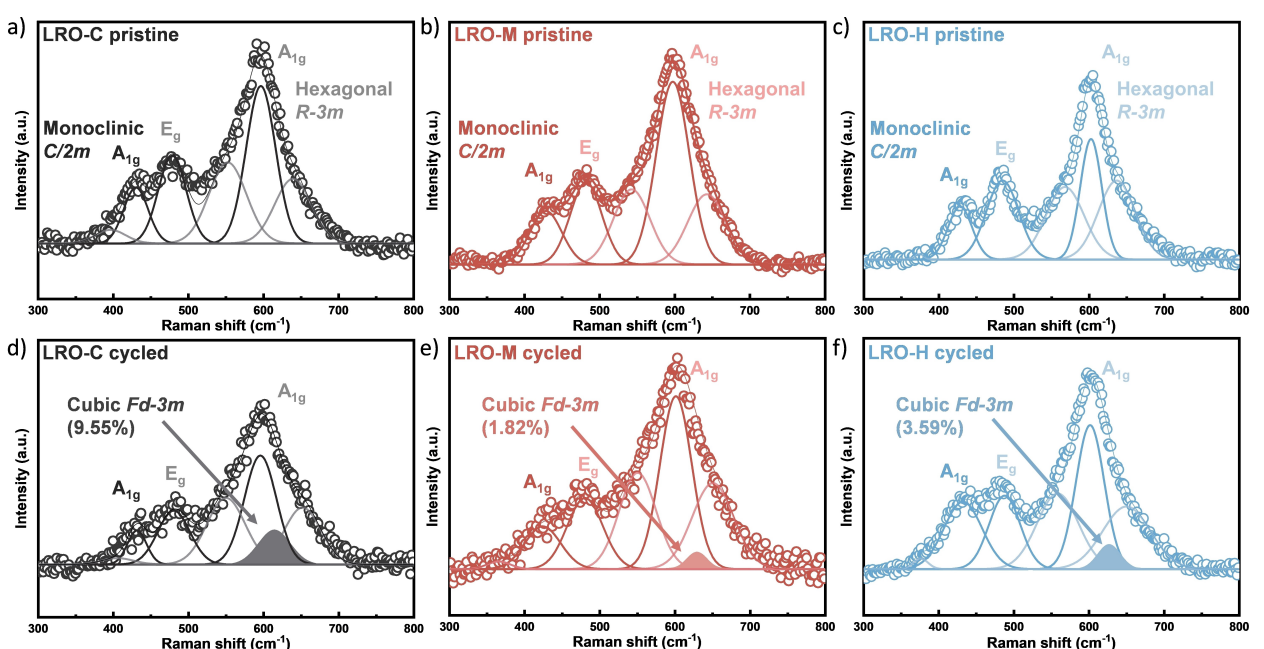


Figure 4. Raman spectra of the a) LRO-C b) LRO-M and c) LRO-H cathodes at the pristine state, and the d) LRO-C, e) LRO-M and f) LRO-H cathodes after 500 cycles.

crystal structures (Figure 4d-f). Nevertheless, the appearance of a peak at about 625 cm^{-1} corresponded to the spinel phase with the $Fd\text{-}3m$ space group,^[42–44] demonstrating inferior layered/spinel phase transition occurred during long-term cycles. The LRO-M electrode exhibited a slight signal of the spinel phase with the fraction of only 1.82%, supporting a relatively stable layered structure can be achieved in the LRO-M, which is beneficial to enhance cyclicity. While both the LRO-C and the LRO-H displayed obvious spinel phases with the fraction of 9.55% and 3.59%, respectively, which directly results in drastic voltage and capacity degradation. These results further demonstrated the choice of appropriate Li source during synthesis process is a crucial factor to improve structural stability. In addition, *ex-situ* SEM characterization was further used to demonstrate the morphology transformation after long cycles (Figure S6). At the pristine state, all cathodes showed the monodisperse primary particles. After 200 and 500 cycles, the three SC cathodes exhibited no obvious crack formation, demonstrating that SC cathodes possess enhanced structural stability compared with PC counterparts.

Conclusions

In summary, we obtained three kinds of SC Li-rich layered oxides by solid-state calcination at high temperature, where Li_2CO_3 , $\text{LiOH}\text{-H}_2\text{O}$ and the mixture of Li_2CO_3 and $\text{LiOH}\text{-H}_2\text{O}$ were acted as Li source mixing with TM hydroxide precursor, respectively. Moreover, *ex-situ* XRD results revealed accelerated phase transition, optimized lithiation speed and particle growth were achieved in the LRO-M during solid-state synthesis process. Furthermore, excellent cycle performance with capacity retention of 84.4% can be obtained within such electrode after 300 cycles, which delivered optimized rate performance, still holding 104.8 mAh g^{-1} at 5 C. In addition, LRO-M proposed superior layered structural stability with limited layered/spinel phase transition of only 1.82%. This study grasps new views and guides into the choice of Li source and optimized design of Li-rich layered cathodes for high-performance Li-ion batteries.

Experimental Section

The details of material synthesis, materials characterization, and electrochemical measurements are given in the Supporting Information.

Author Contributions

Jing Ai and Xiaowen Zhao contributed equally to this work. Xin Cao contributed to the design of the research. Jing Ai carried out the experiments with help from other authors. Xin Cao, Ping Wu and Haoshen Zhou supervised the work. All the authors co-wrote the manuscript, discussed the results, and commented on the manuscript.

Acknowledgements

This work appreciated the financial supports from Natural Science Foundation of Jiangsu Province (BK20230376), National Natural Science Foundation of China (22309085 and 52072181), and Jiangsu Provincial Department of Education (23KJB150019).

Conflict of Interests

The authors declare no conflict of interest.

Data Availability Statement

The date of this work is available from the corresponding author on reasonable request.

Keywords: Lithium-rich layered oxide • Single-crystalline • Solid-state reactions • Growth process • Lithium sources

- [1] M. Armand, J. M. Tarascon, *Nature* **2008**, *451*, 652.
- [2] J. Hong, H. Gwon, S. K. Jung, K. Ku, K. Kang, *J. Electrochem. Soc.* **2015**, *162*, A2447.
- [3] C. Yin, L. Wan, B. Qiu, F. Wang, W. Jiang, H. Cui, J. Bai, S. Ehrlich, Z. Wei, Z. Liu, *Energy Storage Mater.* **2021**, *35*, 388.
- [4] H. Yu, H. Zhou, *J. Phys. Chem. Lett.* **2013**, *4*, 1268.
- [5] J. Zheng, P. Xu, M. Gu, J. Xiao, N. D. Browning, P. Yan, C. Wang, J. G. Zhang, *Chem. Mater.* **2015**, *27*, 1381.
- [6] M. Kotal, S. Jakhar, S. Roy, H. K. Sharma, *J. Energy Storage* **2022**, *47*, 103534.
- [7] W. Fu, Y. Wang, K. Kong, D. Kim, F. Wang, G. Yushin, *Nanoenergy Adv.* **2023**, *3*, 138.
- [8] J. Li, C. Lin, M. Weng, Y. Qiu, P. Chen, K. Yang, W. Huang, Y. Hong, J. Li, M. Zhang, C. Dong, W. Zhao, Z. Xu, X. Wang, K. Xu, J. Sun, F. Pan, *Nat. Nanotechnol.* **2021**, *16*, 599.
- [9] S. Hu, A. S. Pillai, G. Liang, W. K. Pang, H. Wang, Q. Li, Z. Guo, *Electrochem. Energy Rev.* **2019**, *2*, 277.
- [10] S. Cui, M. Gao, G. Li, X. Gao, *Adv. Energy Mater.* **2022**, *12*, 2003885.
- [11] C. Müller, Z. Wang, A. Hofmann, P. Stüble, X. Liu-Théato, J. Klemens, A. Smith, *Batteries & Supercaps* **2023**, *6*, e202300322.
- [12] Q. Shen, R. Zheng, Y. Lv, Y. Lou, L. Shi, S. Yuan, *Batteries & Supercaps* **2022**, *5*, e202200186.
- [13] J. Song, G. Yoon, B. Kim, D. Eum, H. Park, D. Kim, K. Kang, *Adv. Energy Mater.* **2020**, *10*, 2001207.
- [14] D. H. Seo, J. Lee, A. Urban, R. Malik, S. Kang, G. Ceder, *Nat. Chem.* **2016**, *8*, 692.
- [15] X. Zhao, X. Cao, C. Sheng, L. Xu, P. Wu, Y. Zhou, P. He, Y. Tang, H. Zhou, *ACS Appl. Mater. Interfaces* **2024**, *16*, 24147.
- [16] J. Sun, X. Cao, H. Yang, P. He, M. A. Dato, J. Cabana, H. Zhou, *Angew. Chem. Int. Ed.* **2022**, *61*, e202207225.
- [17] J. Sun, C. Sheng, X. Cao, P. Wang, P. He, H. Yang, Z. Chang, X. Yue, H. Zhou, *Adv. Funct. Mater.* **2022**, *32*, 2110295.
- [18] Y. Su, M. Wang, M. Zhang, L. Chen, N. Li, L. Chen, Y. Chen, J. Liu, Y. Li, *J. Alloys Compd.* **2022**, *905*, 164204.
- [19] L. Wang, L. Xu, W. Xue, Q. Fang, H. Liu, Y. Liu, K. Zhou, Y. Li, X. Wang, X. Wang, X. Yang, X. Yu, X. Wang, *Nano Energy* **2024**, *121*, 109241.
- [20] K. Liu, Q. Zhang, Z. Lu, H. Zhu, M. Song, L. Chen, C. Zhang, W. Wei, *ACS Appl. Mater. Interfaces* **2024**, *16*, 14902.
- [21] G. Ding, M. Yao, J. Li, T. Yang, Y. Zhang, K. Liu, X. Huang, Z. Wu, J. Chen, Z. Wu, J. Du, C. Rong, Q. Liu, W. Zhang, F. Cheng, *Adv. Energy Mater.* **2023**, *13*, 2300407.
- [22] S. Burke, J. Whitacre, *Electrochim. Commun.* **2023**, *157*, 107617.
- [23] A. M. Pillai, P. S. Salini, B. John, V. S. Nair, K. Jalaja, S. SarojiniAmma, M. T. Devassy, *Ionics* **2022**, *28*, 5005.
- [24] F. Cao, W. Zeng, J. Zhu, J. Xiao, Z. Li, M. Li, R. Qin, T. Wang, J. Chen, X. Yi, J. Wang, S. Mu, *Small* **2022**, *18*, 2200713.

- [25] C. H. Shen, Q. Wang, F. Fu, L. Huang, Z. Lin, S. Y. Shen, H. Su, X. M. Zheng, B. B. Xu, J. T. Li, S. G. Sun, *ACS Appl. Mater. Interfaces* **2014**, *6*, 5516.
- [26] B. Çetin, Z. Camtakan, N. Yuca, *Mater. Lett.* **2020**, *273*, 127927.
- [27] Z. Wei, Z. Shi, X. Wen, X. Li, B. Qiu, Q. Gu, J. Sun, Y. Han, H. Luo, H. Guo, Y. Xia, C. Yin, P. Cai, Z. Liu, *Mater. Today Energy* **2022**, *27*, 101039.
- [28] J. Hwang, S. Myeong, E. Lee, H. Jang, M. Yoon, H. Cha, J. Sung, M. G. Kim, D. Seo, J. Cho, *Adv. Mater.* **2021**, *33*, 2100352.
- [29] M. Yoon, Y. Dong, Y. Huang, B. Wang, J. Kim, J. S. Park, J. Hwang, J. Park, S. J. Kang, J. Cho, J. Li, *Nat. Energy* **2023**, *8*, 482.
- [30] K. Cao, T. Shen, K. Wang, D. Chen, W. Wang, *Ceram. Int.* **2017**, *43*, 8694.
- [31] J. Mao, J. Iocozzia, J. Huang, K. Meng, Y. Lai, Z. Lin, *Energy Environ. Sci.* **2024**, *17*, 4634.
- [32] J. Sun, X. Cao, W. Yang, E. Yoo, H. Zhou, *J. Mater. Chem. A* **2023**, *11*, 13956.
- [33] Y. Zhang, C. Yin, B. Qiu, G. Chen, Y. Shang, Z. Liu, *Energy Storage Mater.* **2022**, *53*, 763.
- [34] W. Hua, M. Chen, B. Schwarz, M. Knapp, M. Bruns, J. Barthel, X. Yang, F. Sigel, R. Azmi, A. Senyshyn, A. Missiul, L. Simonelli, M. Etter, S. Wang, X. Mu, A. Fiedler, J. R. Binder, X. Guo, S. Chou, B. Zhong, S. Indris, H. Ehrenberg, *Adv. Energy Mater.* **2019**, *9*, 1803094.
- [35] W. Hua, S. Wang, M. Knapp, S. J. Leake, A. Senyshyn, C. Richter, M. Yavuz, J. R. Binder, C. P. Grey, H. Ehrenberg, S. Indris, B. Schwarz, *Nat. Commun.* **2019**, *10*, 5365.
- [36] J. Bai, W. Sun, J. Zhao, D. Wang, P. Xiao, J. Y. P. Ko, A. Huq, G. Ceder, F. Wang, *Chem. Mater.* **2020**, *32*, 9906.
- [37] J. Song, F. Ning, Y. Zuo, A. Li, H. Wang, K. Zhang, T. Yang, Y. Yang, C. Gao, W. Xiao, Z. Jiang, T. Chen, G. Feng, D. Xia, *Adv. Mater.* **2023**, *35*, 2208726.
- [38] Q. Li, D. Ning, D. Wong, K. An, Y. Tang, D. Zhou, G. Schuck, Z. Chen, N. Zhang, X. Liu, *Nat. Commun.* **2022**, *13*, 1123.
- [39] T. Liu, J. Liu, L. Li, L. Yu, J. Diao, T. Zhou, S. Li, A. Dai, W. Zhao, S. Xu, Y. Ren, L. Wang, T. Wu, R. Qi, Y. Xiao, J. Zheng, W. Cha, R. Harder, I. Robinson, J. Wen, J. Lu, F. Pan, K. Amine, *Nature* **2022**, *606*, 305.
- [40] M. Farahmandjou, W. Lai, J. Safaei, S. Wang, Z. Huang, F. Marlton, J. Ruan, B. Sun, H. Gao, K. Ostrikov, P. H. L. Notten, G. Wang, *Batteries & Supercaps* **2023**, *6*, e202300123.
- [41] R. A. House, J. J. Marie, M. A. Pérez Osorio, G. J. Rees, E. Boivin, P. G. Bruce, *Nat. Energy* **2021**, *6*, 781.
- [42] B. Zhang, Y. Zhang, X. Wang, H. Liu, Y. Yan, S. Zhou, Y. Tang, G. Zeng, X. Wu, H. G. Liao, Y. Qiu, H. Huang, L. Zheng, J. Xu, W. Yin, Z. Huang, Y. Xiao, Q. Xie, D. L. Peng, C. Li, Y. Qiao, S. G. Sun, *J. Am. Chem. Soc.* **2023**, *145*, 8700.
- [43] B. Zhang, H. Zhang, H. Luo, H. Hua, X. Wu, Y. Chen, S. Zhou, J. Yin, K. Zhang, H. Liao, Q. Wang, Y. Zou, Y. Qiao, S. Sun, *Angew. Chem. Int. Ed.* **2024**, *63*, e202316790.
- [44] B. Chen, B. Zhao, J. Zhou, J. Song, Z. Fang, J. Dai, X. Zhu, Y. Sun, *J. Solid State Electrochem.* **2018**, *22*, 2587.

Manuscript received: June 27, 2024

Revised manuscript received: July 28, 2024

Accepted manuscript online: July 31, 2024

Version of record online: September 25, 2024